

Quantum effects in muon spin spectroscopy within the stochastic self-consistent harmonic approximation

Ifeanyi John Onuorah,^{1,*} Pietro Bonfà,¹ Roberto De Renzi,^{1,†} Lorenzo Monacelli,² Francesco Mauri,² Matteo Calandra,³ and Ion Errea^{4,5,6}

¹*Department of Mathematical, Physical and Computer Sciences, University of Parma, Italy*

²*Dipartimento di Fisica, Università di Roma Sapienza, Italy*

³*Sorbonne Université, CNRS, Institut des Nanosciences de Paris, UMR7588, F-75252 Paris, France*

⁴*Fisika Aplikatua 1 Saila, Gipuzkoako Ingeniaritza Eskola,*

University of the Basque Country (UPV/EHU), Donostia-San Sebastian, Basque Country, Spain

⁵*Centro de Física de Materiales (CSIC-UPV/EHU), Donostia-San Sebastian, Basque Country, Spain*

⁶*Donostia International Physics Center (DIPC), Donostia-San Sebastian, Basque Country, Spain*

(Dated: April 29, 2019)

In muon spin rotation experiments the positive implanted muon vibrates with large zero point amplitude by virtue of its light mass. Quantum mechanical calculations of the host material usually treat the muon as a point impurity, ignoring this large vibrational amplitude. As a first order correction, the muon zero point motion is usually described within the harmonic approximation, despite the large anharmonicity of the crystal potential. Here we apply the stochastic self-consistent harmonic approximation, a quantum variational method devised to include strong anharmonic effects in total energy and vibrational frequency calculations, in order to overcome these limitations and provide an accurate *ab initio* description of the quantum nature of the muon. We applied this full quantum treatment to the calculation of the muon contact hyperfine field in textbook-case metallic systems, such as Fe, Ni, Co including MnSi and MnGe, significantly improving agreement with experiments. Our results show that muon vibrational frequencies are strongly renormalized by anharmonicity. Finally, in contrast to the harmonic approximation, we show that including quantum anharmonic fluctuations, the muon stabilizes at the octahedral site in bcc Fe.

I. INTRODUCTION

Muon spin spectroscopy (μ SR) relies on positive muons (anti-muons) implanted in a regime of extreme dilution at *a priori* unknown crystal interstitial sites. The muon spin dynamics is recorded just after its implantation in the material under investigation over a time range of a few microseconds, which makes μ SR, among other things, a technique of election for the investigation of magnetic properties in condensed matter.

An accurate, *ab initio*, description of the electron-muon interaction in periodic solids has been out of reach until a few years ago. The dramatic increase of both the computational power and the accuracy of first principles calculations make this goal possible. Self-consistent electronic structure calculations, in particular those based on density functional theory (DFT), are already employed to study the muon implantation site, muon interaction parameters, and for understanding the muon induced distortion in the lattice [1–7]. This turns out to be a very valuable tool for analyzing experimental data and interpreting the results. The knowledge of the muon implantation site(s) and of the hyperfine field allows very important quantitative information, including the magnetic structure and the moment size, to be obtained from μ SR experiments. Moreover, a reliable quantum calculation

of the muon embedded in the system under investigation provides an estimate for its induced perturbation; the probe is an impurity and it may in principle alter the local electronic properties. Fortunately this is a very rare case, and yet assessing these rare cases [8, 9] is very important.

However, self-consistent DFT calculations often treat the muon as just another atom in the lattice, within the Born-Oppenheimer (BO) approximation [10], without taking into consideration the quantum effect of the sizeable muon zero point vibration (ZPV). The embedded muon, by virtue of its very light mass ($\sim 1/9^{th}$ the proton mass), is characterized by a large zero-point amplitude and the spread of the muon wavefunction is typically in the order of 1 Bohr radius. The neglect of this factor may have two major consequences: inaccurate estimation of the contact hyperfine field, and/or incorrect identification of muon implantation sites. The former is due to neglect of the space extent of the muon wavefunction, whereas the latter happens when the inclusion of the quantum ZPV in the energetics changes the relative stability of different implantation sites.

Earlier approaches towards the quantum mechanical description of the muon ZPV include calculations within the harmonic approximation [3, 11]. However, the muon potential has been discussed and shown to be anharmonic, for instance by total energy calculations with site exploration algorithms [1, 12–14]. Furthermore, break down of the harmonic approximation takes place when within the range of the muon vibrations the potential is not represented by the second-order term in its Taylor

* ifeanyijohn.onuorah@unipr.it

† roberto.derenzi@unipr.it

expansion.

Alternative methods do take into account the anharmonic nature of the crystalline potential. One of them consists in the potential exploration approach (PEA) within a double Born-Oppenheimer approximation [14]. The non BO methods represent another computationally very intensive alternative, employing linear combination of Gaussian basis functions to realize both the nuclear and the electronic degrees of freedom [15–18] and optimized local potentials to represent the nuclear-electron correlation [19]. One of the most advanced approach relies on path integral molecular dynamics (PIMD), which allows for contextual quantization of both the muon and the electrons in the calculation of the electronic structure and of the interatomic forces [13, 20, 21]. However, computational resources required by this method grow exceedingly with the size of the cell.

In this paper, we describe a stochastic self-consistent harmonic approximation (SSCHA) that allows to include the effects of anharmonicity in the muon vibrations [22–25]. The SSCHA is a quantum variational method that efficiently calculates anharmonic free energies and phonon frequencies in a non-perturbative way. This approach has been very successful for calculating phonon frequencies and superconducting properties in hydrogen-rich materials, as well as in systems undergoing charge density wave (CDW) transitions, ferroelectrics, and thermoelectrics [22, 26–31]. For the muon, the SSCHA is variational in the muon (free) energy, with this energy evaluated stochastically from forces and energies calculated at a sufficient number of random muon configurations. The muon energy is minimized using trial harmonic wave functions that are Gaussian while the minimization parameter is the width of the Gaussian. From the output of the minimization, renormalized anharmonic muon frequencies and the muon ground state energy can be extracted.

With this approach, we demonstrate that huge anharmonicity renormalizes significantly the harmonic muon vibrational modes, as expected for the muon due to its light mass. We further use the SSCHA muon wavefunction to recalculate the contact hyperfine field in a series of metals: Fe, Ni, Co, MnSi and MnGe, where SSCHA improves the agreement of the calculated value with the experimental results, with respect to recent point impurity calculations [6]. The SSCHA together with energy curvature considerations [24] allows the stable occupation of the muon at the octahedral site in bcc Fe, that is unstable within the harmonic regime.

The paper has the following structure: Sec. II discusses the double Born-Oppenheimer approximation that allows to separate the muon degrees of freedom from those of the host nuclei and electrons. In Sec. III, we describe the working principles of the SSCHA including the stochastic implementation. In Sec. IV we discuss the muon zero point energy (ZPE) calculation results using the SSCHA together with the stability of the muon at octahedral and tetrahedral sites in Fe(bcc). Finally, in Sec. V we present

the results of the quantum corrections in the calculation of the contact hyperfine field and then conclusions in Sec. VI.

II. DOUBLE BORN-OPPENHEIMER APPROXIMATION

The BO approximation considers the nuclei frozen on the time scale of electron dynamics in view of their sufficiently large mass ratio [10]. Hydrogen is already sufficiently lighter than most other atoms to allow a further separation of time scales, and this holds *a fortiori* true for a positive muon. This allows for the quantum treatment of a single muon *impurity* in the crystal by employing the so-called Double Born-Oppenheimer approximation (DBO) [12, 14, 32]. The muon dynamics ($m_\mu \sim 200m_e$) is much slower than that of electrons, thus justifying an electron structure obtained by DFT with frozen muon and nuclei. The same muon dynamics is still much faster than that of other nuclei, since transition metals are typically 400 times heavier than a muon (care must be taken when considering e.g. hydrogen, only 9 times heavier than a muon). Therefore it is justified to use total DFT energy vs. the muon configuration coordinates as a frozen potential energy landscape in which the muon dynamics takes place on its characteristic time scale. This allows to consider the zero-point vibration of only the muon within the potential energy surface (PES), drastically reducing the computational load requirements for the calculations.

The total Hamiltonian H_{tot} describing the many body interaction including explicitly the muon coordinates is written as

$$H_{tot} = T_e + T_\mu + T_N + V(\mathbf{r}_e, \mathbf{r}_\mu, \mathbf{R}_N), \quad (1)$$

with subscript μ describing the muon related quantities while e and N describe those of the electrons and host nuclei respectively. T and V are the kinetic and potential energy respectively. The Schrödinger equation is then written as

$$H_{tot} |\Psi_{tot}\rangle = E_{tot} |\Psi_{tot}\rangle. \quad (2)$$

This further allows to write the DBO wavefunction as a product wavefunction of the electrons, the muon and the nuclei in the form:

$$|\Psi_{tot}\rangle = |\psi_e\rangle |\phi_\mu\rangle |\Phi_N\rangle. \quad (3)$$

The Hamiltonian for the electronic problem can be rewritten to specifically point out the presence of the muon position operator as

$$H_e = T_e + V(\mathbf{r}_e; \mathbf{r}_\mu, \mathbf{R}_N). \quad (4)$$

Similar to the BO approximation, only the position operators of the muon and the nuclei enter in the eigenvalue problem of the electrons. The solution of the electronic

problem gives the BO PES, $V(\mathbf{r}_\mu, \mathbf{R}_N)$ dependent on the muon and the nuclei position operators.

Hence, the ground state Hamiltonian H_μ for the muon can be written as

$$H_\mu = T_\mu + V(\mathbf{r}_\mu; \mathbf{R}_N), \quad (5)$$

where the muon kinetic energy T_μ is defined as

$$T_\mu = \sum_{\lambda=1}^3 \frac{p_\lambda^2}{2m_\mu}$$

with p the momentum operator along the Cartesian component indexes λ , while m_μ is the muon mass.

The acquisition of the DBO PES $V(\mathbf{r}_\mu; \mathbf{R}_N)$ for the solution of the Schrödinger equation Eq. 5, is still a long and difficult task. However, the DBO approximation is advantageous since it allows to consider separately only the degrees of freedom relating to the muon, thus understanding the true muon motion behaviour. It also saves a lot of computational effort, time and resources as will be described in the next section.

III. STOCHASTIC SELF-CONSISTENT HARMONIC APPROXIMATION (SSCHA) FOR MUONS

The DBO approximation greatly alleviates the computational effort required within SSCHA by reducing the number of considered degrees of freedom. The burden is due to the number of irreducible modes quickly growing with the large size of the supercell containing one muon impurity, which is required to avoid artificial interactions among muon periodic replica. In the DBO frame it is justified to limit the anharmonic treatment to the degrees of freedom involving the muon, keeping heavier nuclei, 3d elements, Si or Ge fixed in the SSCHA calculations. This consideration is supported by the evolution of the eigenfrequencies in a *full* SSCHA calculation including anharmonic effects both for the Fe host nuclei and the muon at the tetrahedral site. Figure 1 shows that muon eigenfrequencies are largely renormalized after several iterations, whereas the lower frequency modes of the heavier Fe nuclei are barely affected. The calculation is performed with a $2 \times 2 \times 2$ supercell.

To continue with the formal description of the SSCHA restricted to the muon modes, we can write the muon Hamiltonian H_μ simply as H , the muon wavefunction ϕ_μ as ϕ and the DBO potential energy surface $V(\mathbf{r}_\mu; \mathbf{R}_N)$ as $V(\mathbf{r}_\mu)$, since the interest here is on a potential for the muon influenced only by changes in the muon degrees of freedom.

The muon ZPE from the Hamiltonian H is given as

$$E = \langle \phi | H | \phi \rangle, \quad (6)$$

where $|\phi\rangle$ is the muon ground state wavefunction. Calculating E is far from trivial since the form of the muon

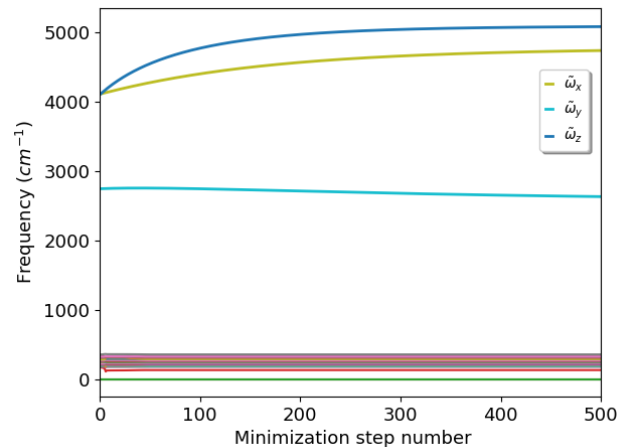


FIG. 1. Evolution of the SSCHA muon frequency ($\tilde{\omega}$) and those of Fe (nearly static low frequency lines in red-like and green colours) during minimization for muon in tetrahedral site of bcc Fe starting from the harmonic ones. The figure depicts the expected strong anharmonicity effects on the SSCHA muon frequencies and nearly non-existent anharmonicity effects on those of Fe, due to the large mass difference of the muon and Fe nuclei. The muon is ≈ 490 times lighter.

potential (Eq. 5) is not known. However, it is possible to establish a quantum variational principle for the muon ground state energy E , by replacing the exact muon wavefunction $|\phi\rangle$ with the wavefunction $|\tilde{\phi}\rangle$ of a trial muon Hamiltonian $\tilde{H} = T_\mu + \tilde{V}(\mathbf{r}_\mu)$ with energy

$$\tilde{E} = \langle \tilde{\phi} | \tilde{H} | \tilde{\phi} \rangle. \quad (7)$$

This is such that one can define an energy functional of the trial Hamiltonian as

$$\tilde{E}_H[\tilde{H}] = \langle \tilde{\phi} | H | \tilde{\phi} \rangle. \quad (8)$$

The variational form of the muon ground state energy can be written as

$$E \leq \tilde{E}_H[\tilde{H}] \quad (9)$$

such that the equality holds when the true and trial potentials are the same.

By adding and subtracting Eq. 7 to Eq. 8, $\tilde{E}_H[\tilde{H}]$ is written in the form

$$\tilde{E}_H[\tilde{H}] = \tilde{E} + \langle \tilde{\phi} | (V - \tilde{V}) | \tilde{\phi} \rangle. \quad (10)$$

The above definitions allow to formulate a variational principle following the Gibbs-Bogoliubov inequality theorem [33] at zero temperature, similar to the Rayleigh-Ritz inequality [34].

According to the trial wave function, the probability to find the muon in the position \mathbf{r}_μ is

$$\tilde{\rho}(\mathbf{r}_\mu) = \langle \mathbf{r}_\mu | \tilde{\phi} \rangle \langle \tilde{\phi} | \mathbf{r}_\mu \rangle = |\tilde{\phi}(\mathbf{r}_\mu)|^2. \quad (11)$$

Thus, an observable A dependent only on \mathbf{r}_μ can be averaged statistically within the form of the corresponding Hamiltonian \tilde{H} as

$$\langle A \rangle_{\tilde{H}} = \int d\mathbf{r}_\mu A(\mathbf{r}_\mu) \tilde{\rho}(\mathbf{r}_\mu) \quad (12)$$

and the muon energy in Eq. 10 can be evaluated as

$$\tilde{E}_H[\tilde{H}] = \tilde{E} + \int d\mathbf{r}_\mu \tilde{\rho}(\mathbf{r}_\mu) (V(\mathbf{r}_\mu) - \tilde{V}(\mathbf{r}_\mu)). \quad (13)$$

With the above form of $\tilde{E}_H[\tilde{H}]$, the muon energy can be evaluated at each step during the variational minimization. One can directly see that the equality in the form of the variation in Eq. 9 holds if $V = \tilde{V}$. Hence, with the variational principle, the ground state of the muon is determined if the potential $\tilde{V}(\mathbf{r}_\mu)$ that minimizes $\tilde{E}_H[\tilde{H}]$ is found.

A. Variational potential

The variational inequality of Eq. 9 holds for any \tilde{V} potential. However, in the SSCHA a trial harmonic potential is chosen. The choice of a trial harmonic potential is very convenient because we can exploit the fact that its wavefunction is a Gaussian with a known analytic expression for the energy \tilde{E} . This simplifies a lot the problem, as computing the energy accounts for the most time consuming part in other self-consistent methods including Hartree-Fock or DFT methods. Also, the Gaussian allows to extract randomly distributed configurations without any Metropolis algorithm that requires long equilibration times. The Gaussian wave functions approximate the real wave functions. It should not be confused that this trial potential is not the harmonic potential obtained from the second derivatives of V at the minimum.

The trial muon harmonic Hamiltonian is thus of the form

$$\tilde{H} = \sum_{\lambda=1}^3 \frac{p_\lambda^2}{2m_\mu} + \frac{1}{2} \sum_{\lambda\nu} K^{\lambda\nu} (r_\mu - r_\mu^{eq})^\lambda (r_\mu - r_\mu^{eq})^\nu, \quad (14)$$

where λ and ν are Cartesian component indexes, \mathbf{r}_μ^{eq} is the muon equilibrium position, m_μ is the mass of the muon and $K^{\lambda\nu}$ is the muon 3×3 force constant matrix. The force constant matrix $K^{\lambda\nu}/m_\mu$ can be constructed and diagonalized as

$$\sum_{\nu=1}^3 \frac{K^{\lambda\nu}}{m_\mu} \tilde{\epsilon}_i^\nu = \tilde{\omega}_i^2 \tilde{\epsilon}_i^\lambda, \quad (15)$$

where i is the index of each of the orthogonal modes, $\tilde{\epsilon}_i^\nu$ is the polarization vector and $\tilde{\omega}_i$ is the muon frequency corresponding to the trial Hamiltonian \tilde{H} for each mode.

Assuming a trial harmonic potential, the probability to find the muon at \mathbf{r}_μ can be written simply as

$$\tilde{\rho}(\mathbf{r}_\mu) = \frac{1}{\prod_{i=1}^3 \sqrt{2\pi\tilde{\sigma}_i^2}} \exp\left(-\sum_{\lambda\nu i} \frac{\tilde{\epsilon}_i^\lambda \tilde{\epsilon}_i^\nu}{2\tilde{\sigma}_i^2} (r_\mu - r_\mu^{eq})^\lambda (r_\mu - r_\mu^{eq})^\nu\right), \quad (16)$$

where $\tilde{\sigma}_i$, the normal length for each of the mode i , is given as

$$\tilde{\sigma}_i = \sqrt{\frac{\hbar}{2m_\mu \tilde{\omega}_i}}. \quad (17)$$

If the probability density is defined, using the quantum statistical averaging already defined in Eq. 12, the energy of the trial harmonic Hamiltonian can be calculated as

$$\tilde{E} = \sum_{i=1}^3 \frac{1}{2} \hbar \tilde{\omega}_i. \quad (18)$$

B. Energy minimization and stochastic implementation

From the variational principle already discussed above, the ground state muon energy is achieved by a conjugate gradient (CG) minimization algorithm [35]. At the minimum,

$$E^{anh} = \min \tilde{E}_H[\tilde{H}] \quad (19)$$

is the vibrational ZPE of the muons. The $\tilde{\omega}_i$ phonons obtained diagonalizing K at the minimum should be understood as the muon frequencies that parameterize the ground state variational muon wavefunction. In order to obtain physical phonons, the second derivative (curvature) of E^{anh} with respect to \mathbf{r}_μ has to be calculated [24], which includes a correction term to the force constants matrix $K^{\lambda\nu}/m_\mu$ in Eq. 15. We verified that for the cases under study here the muon frequencies are affected by less than a 1% by this extra correction. Thus, we will treat in the following the $\tilde{\omega}_i$ frequencies as the physical vibrational energies of the muons.

If the *equilibrium* implantation site of the muon \mathbf{r}_μ^{eq} is known and also remains fixed by symmetry, for example when muons occupy symmetrical octahedral and tetrahedral interstitial positions in cubic systems, minimizing $\tilde{E}_H[\tilde{H}]$ with respect to the trial potential \tilde{V} is similar to minimizing it with respect to the force constant matrix $K^{\lambda\nu}$. Hence, the muon energy is only minimized with respect to the force constant matrix K . For the muon in a high symmetry position, the force constant matrix is a 3×3 matrix, with the diagonal elements of the matrix accounting for the dominant contribution. However, if the equilibrium position of the muon is not precisely known and perhaps not at a high symmetry position, the muon energy can also be minimized with respect to the muon

TABLE I. Harmonic muon frequencies ω_i^h along the mode i and harmonic ZPE $E^h = \sum_{i=1}^3 \hbar\omega_i^h/2$, together with the SSCHA muon frequencies $\tilde{\omega}_i$ at the minimum as well as the muon vibrational energy E^{anh} that includes the anharmonic contribution.

| Host | ω_x^h (cm ⁻¹) | ω_y^h (cm ⁻¹) | ω_z^h (cm ⁻¹) | E^h (eV) | $\tilde{\omega}_x$ (cm ⁻¹) | $\tilde{\omega}_y$ (cm ⁻¹) | $\tilde{\omega}_z$ (cm ⁻¹) | E^{anh} (eV) |
|-----------------------|----------------------------------|----------------------------------|----------------------------------|--------------|--|--|--|----------------|
| Fe - bcc ^a | 4364.01 | 2913.01 | 4364.62 | 0.72 | 4769.08 | 2572.58 | 5088.37 | 0.74 |
| Fe - bcc ^b | 1965.08 <i>i</i> | 1958.72 <i>i</i> | 6828.00 | ^c | 2005.24 | 2005.24 | 6364.81 | 0.53 |
| Co - hcp | 2930.41 | 2929.85 | 2752.25 | 0.53 | 3741.10 | 3741.10 | 3476.24 | 0.61 |
| Co - fcc | 2607.29 | 2607.02 | 2606.66 | 0.49 | 3424.16 | 3424.16 | 3424.16 | 0.56 |
| Ni - fcc | 2377.62 | 2377.60 | 2377.61 | 0.44 | 3317.78 | 3317.78 | 3317.78 | 0.53 |
| MnGe | 3123.70 | 3123.67 | 3123.66 | 0.58 | 3470.29 | 3470.29 | 3470.29 | 0.64 |
| MnSi | 3296.27 | 3296.32 | 3296.11 | 0.61 | 3685.25 | 3685.25 | 3685.25 | 0.67 |

^a Muon at tetrahedral site

^b Muon at octahedral site

^c The muon is not stable at the octahedral site (imaginary frequencies) within the harmonic regime.

position, such that the \mathbf{r}_μ and $K^{\lambda\nu}$ that minimizes $\tilde{E}_H[\tilde{H}]$ are those of the ground state [23, 25]. Calculations and results reported in this work do not include minimization with respect to \mathbf{r}_μ , since at the moment the interest is on materials where there is sufficient knowledge of the equilibrium muon site. However, we verified with SSCHA that the muon remains locked at the equilibrium position within stochastic error.

A very important quantity required for the CG minimization is the gradient of the energy $\nabla_K \tilde{E}_H[\tilde{H}]$ with respect to the force constant K . The analytic form is written as (See Ref. [23])

$$\nabla_K \tilde{E}_H[\tilde{H}] = - \sum_{i\lambda\nu} (\tilde{c}_i^\lambda \nabla_K \ln \tilde{\sigma}_i + \nabla_K \tilde{c}_i^\lambda) \tilde{c}_i^\nu \times \int d\mathbf{r}_\mu [f^\lambda(\mathbf{r}_\mu) - \tilde{f}^\lambda(\mathbf{r}_\mu)] (r_\mu - r_\mu^{eq})^\nu \tilde{\rho}(\mathbf{r}_\mu), \quad (20)$$

where $f^\lambda(\mathbf{r}_\mu)$ is the muon force component in the direction of the Cartesian indexes λ for all muon positions \mathbf{r}_μ and $\tilde{f}^\lambda(\mathbf{r}_\mu)$ are the forces obtained with the \tilde{V} potential. The SSCHA minimization is performed respecting the symmetries of the crystal [23].

In principle, in order to obtain the forces for solving the gradient, high order terms which are intensive to calculate are required [36–38]. However, this is avoided by a stochastic sampling helped by the known analytic form of $\tilde{\rho}(\mathbf{r}_\mu)$ together with importance sampling and re-weighting techniques. The stochastic sampling is advantageous because it allows the system to be minimized farther away from the starting potential without the loss of accuracy unlike the PES fit methods that enforce the solution to remain close to the starting point.

For an operator A that depends on the muon position, its quantum statistical average can be calculated by averaging the operator over sufficiently large number of configurations, N_c . Thus, the statistical average Eq. 12 is performed stochastically over N_c random configuration in the form

$$\int d\mathbf{r}_\mu A(\mathbf{r}_\mu) \tilde{\rho}_0(\mathbf{r}_\mu) \simeq \frac{1}{N_c} \sum_{n=1}^{N_c} A(\mathbf{r}_\mu^n) \equiv \langle A \rangle_{\tilde{H}_0}. \quad (21)$$

Here, \tilde{H}_0 is the starting trial Hamiltonian at CG step $j = 0$. The N_c random muon configurations are generated by making use of random numbers $\{\xi_{in}\}_{n=1,\dots,N_c}$ created with the Gaussian distribution of $\tilde{\rho}(\mathbf{r}_\mu)$ and rescaled by the corresponding normal length modes $\tilde{\sigma}_i \xi_{in}$ and polarization vector \tilde{c}_i^λ . As already discussed, the host nuclei are kept fixed and the random muon position configurations have the following distribution:

$$(r_\mu^n)^\lambda = (r_\mu^{eq})^\lambda + \sum_{i=1}^3 \tilde{c}_i^\lambda \tilde{\sigma}_i \xi_{in}. \quad (22)$$

For each of the N_c configuration, the forces on the muon $\mathbf{f}(\mathbf{r}_\mu)$ and the BO energy \tilde{V} due to the muon displacement are calculated. These are used for the stochastic statistical averaging in the gradient evaluation (Eq. 20) and the energy (Eq. 13). The forces and energies can be calculated outside the SSCHA with any of *ab initio* method including DFT [39] and Hartree-Fock [40–42] methods.

Calculation of the forces and energy for the N_c configuration accounts for the most computationally demanding task in the SSCHA minimization cycle. After the first step in the CG minimization, these force and energy calculations are circumvented by a reweighting procedure at each step for $j > 0$ in the minimization cycle, considering that hundreds of step are required before the minimum is found. The reweighting procedure involves multiplying the importance sampled integral Eq. 21 at each step j by a factor $\wp(\mathbf{r}_\mu^n)$ defined as

$$\wp(\mathbf{r}_\mu^n) = \frac{\tilde{\rho}_j(\mathbf{r}_\mu^n)}{\tilde{\rho}_0(\mathbf{r}_\mu^n)} \quad (23)$$

such that for each step j in the CG minimization, the muon energy $\tilde{E}_H(\tilde{H})$ and the energy gradient $\nabla_K \tilde{E}_H(\tilde{H})$ are averaged statistically by importance sampling and reweighting techniques as

$$\int d\mathbf{r}_\mu A(\mathbf{r}_\mu) \tilde{\rho}_j(\mathbf{r}_\mu) \simeq \frac{1}{N_c} \sum_{n=1}^{N_c} A(\mathbf{r}_\mu^n) \wp(\mathbf{r}_\mu^n) \equiv \langle A \rangle_{\tilde{H}_j} \quad (24)$$

If $j = 0$, $\wp(\mathbf{r}_\mu^n) = 1$. Eq. 24 has *real* effects only for $j > 0$. In Eq. 23, $\tilde{\rho}_j$ is the probability density function with the trial Hamiltonian at step j .

In the minimization cycle, if the reweighting procedure is estimated to be out of range following the criteria in Ref. [25] or if an increase in precision is desired, forces are recalculated with more number of random configurations. The minimization is stopped when the gradient is small enough, ensuring that the $\tilde{\omega}_i$ phonons as well as $\tilde{E}_H[\tilde{H}]$ are converged.

IV. SSCHA MUON FREQUENCIES

With the SSCHA described above, the muon frequencies and the ZPE were calculated for the following metallic systems; Fe, Co, Ni, MnSi, MnGe. The muon contact hyperfine field was already evaluated for these materials [6] treating the muon as a point impurity, i.e. without the ZPV effects.

The harmonic muon frequencies for all the materials considered were calculated by the finite difference method [43, 44], which allows only the muon frequencies to be singled out. These were used for the starting trial potential for the SSCHA minimization except for the stability discussion in Sec. IV A with the muon at the octahedral and tetrahedral site in bcc Fe. Here, the density functional perturbation theory (DFPT) within the Quantum ESPRESSO suite of code [45, 46] was used to calculate the frequencies of the whole system, including those of the host Fe nuclei. The resulting harmonic muon frequencies from both methods in the two Fe systems are in good agreement.

For the minimization and the stochastic averaging (see Eq 21), hundreds (100 to 400) of random configurations were generated for the muon, while keeping the host atoms fixed, to ensure that the muon energy gradient vanishes. Their energies and Hellmann-Feynman forces [47] were calculated by DFT as implemented in the Quantum ESPRESSO suite of code [46]. The details of the muon site in these systems and DFT input parameters are contained in Ref. [6]. For all the systems, a $2 \times 2 \times 2$ supercell constructed starting from the conventional unit cell were used for the harmonic frequency calculations, the SSCHA frequency minimization and the force calculation within DFT. Other DFT computational details are identical to those reported in Ref. [6]. To accommodate the muon impurity in the supercell, the forces introduced by the muon in the system were relaxed by DFT and the relaxed structures were used for the SSCHA calculations.

Figure 2 shows the evolution of the SSCHA muon frequencies and energy during the minimization. Particularly, one observes that the resulting SSCHA frequencies that describe the muon wavefunction are strongly renormalized by anharmonicity. The anharmonic contribution to the change in frequency observed along the modes is in the range of 330 - 820 cm^{-1} . This considerably alters the spread of the muon wavefunction. The stochastic implementation ensures that the effect of the muon vibrations, the effect of the chemical environment around the muon

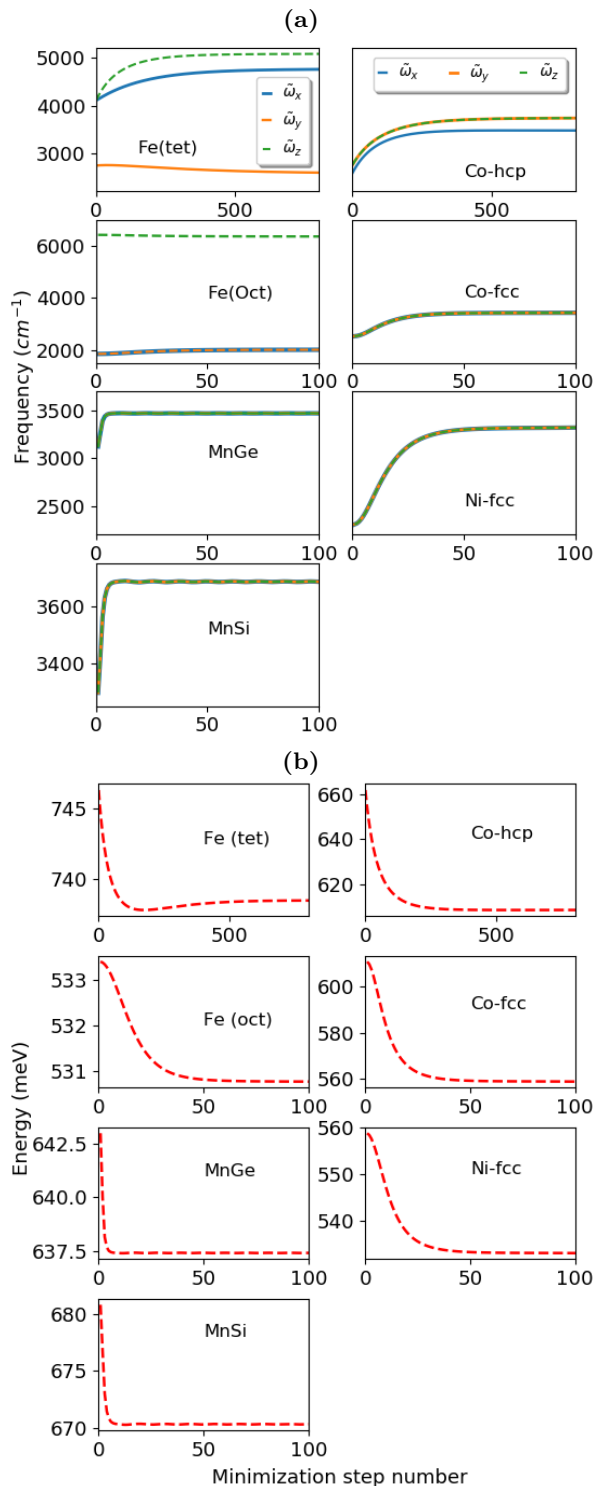


FIG. 2. (a) Evolution of the SSCHA muon frequency during the minimization steps (b) Evolution of SSCHA muon energy as in Eq. 13 during the minimization steps. In both figures the starting point for the minimization step number = 0, is that of the harmonic Hamiltonian except for the muon in octahedral site of Fe (Fe (Oct)) when the starting potential is arbitrary.

and anharmonic contributions to the forces acting on the

muon are all incorporated in the muon ground state minimum.

Table I contains the harmonic frequencies ω_i^h and energies $E^h = \sum_{i=1}^3 \hbar\omega_i^h/2$ together with the SSCHA results at the end of the minimization. The results show the huge anharmonic effects in the muon vibrational frequencies, in particular, for bcc Fe with octahedral implantation site, which is highly unstable in the harmonic approach. For all other cases with positive harmonic frequencies for which E^h can be defined, the difference between the SSCHA muon vibrational energies and the harmonic ones are in the range of 0.02 - 0.09 eV.

A. Tetrahedral and octahedral muon site in Fe

Conflicting experimental and theoretical studies report the muon site in Fe to be either the tetrahedral (T) or the octahedral (O) interstitial sites [48–53]. From the point of view of the total DFT energy, the T site is 0.184 eV lower than the O site. This would indicate that the T site is the stable one, although the small difference with reference to the muon ZPE does not exclude that both may be populated.

DFPT calculations of the muon frequencies provide further insight on the stability of the two candidate sites: unphysical *negative* frequencies generally signal an instability. This is the case for the muon at the O site, as opposed to those of the T site, always positive. The harmonic approximation then appears to indicate instability of the muon at the O site. The instability at the O site remains even when symmetry constraints are released.

However, the anharmonic effects, fully captured by the SSCHA, yield positive frequencies also for the O site indicating that the instability is an artifact of the harmonic approximation. As the $\tilde{\omega}_i$ frequencies are positive definite by definition, this is not a proof that the O site occupation is stable. Obtaining the frequencies from the energy curvature [24], which can correctly describe an instability, confirms however that the O site interstitial site is in fact stable. The SSCHA frequencies for the muon in the O site are larger than the frequencies resulting from those obtained from the curvature by only 0.53 % along the x,y axis and 0.14 % along the z axis.

The quantum correction with SSCHA shows that both T and O turn out to be stable local minima. The vibrational contribution to the energy is 0.21 eV less for the O site than for the T site (see Table I). Adding this to the static DFT contribution makes the O site energetically favored by approximately 0.03 eV over the T site. However, this is a rather small energy difference, and we cannot rule out the occupation of both sites, recalling that the muon implantation process does not necessarily reach true equilibrium.

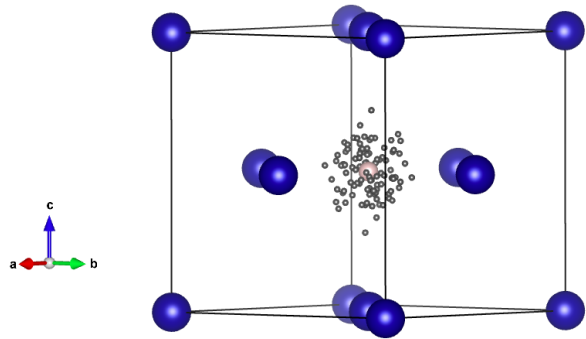


FIG. 3. 100 random position generated using Eq. 22 for the muon at octahedral site in Co-fcc unit cell. The equilibrium octahedral center is depicted by the pink sphere, while the small dark spheres represent the different random muon positions where the muon contact hyperfine field within point impurity treatment $B_c(\mathbf{r}_\mu)$ was also calculated for the purpose of including the quantum effects of the muon.

V. QUANTUM CORRECTIONS ON MUON CONTACT HYPERFINE FIELD

The contact hyperfine field $B_c(\mathbf{r}_\mu)$ at the muon position \mathbf{r}_μ is computed *ab initio* by considering the imbalance in the spin density at the muon site [6] given as

$$B_c(\mathbf{r}_\mu) = \frac{2}{3} \mu_0 \mu_B [n_\uparrow(\mathbf{r}_\mu) - n_\downarrow(\mathbf{r}_\mu)], \quad (25)$$

where μ_0 is the vacuum permeability, μ_B is the Bohr magneton and $n_\uparrow - n_\downarrow$ represents the spin polarization at the muon site \mathbf{r}_μ calculated here by DFT. $B_c(\mathbf{r}_\mu^{eq})$ has been calculated in this way for metals within a point impurity treatment of the muon [6]. We now calculate the effect of the muon quantum delocalization on its contact hyperfine field, using the muon SSCHA wave function ϕ already renormalized by anharmonicity. Its probability density $|\phi(\mathbf{r}_\mu)|^2$ follows the same definition as in Eqs. 11 and 16.

The quantum expectation value, $\langle B_c \rangle$ is given by

$$\langle B_c \rangle = \int d\mathbf{r}_\mu B_c(\mathbf{r}_\mu) |\phi(\mathbf{r}_\mu)|^2 \quad (26)$$

and is evaluated in a post-DFT calculation by a statistical average performed stochastically following Eq. 21, over a number of muon random configuration displaced from the equilibrium position \mathbf{r}_μ^{eq} and generated with the probability distribution of the muon wavefunction (see Eq. 22). The number of configurations used is the same as in the SSCHA minimization of the muon wavefunction. However, the new muon random positions are generated considering the anharmonic corrected SSCHA muon wavefunction. Figure 3 shows the distribution of the 100 muon configurations used for fcc Co in the unit cell.

$B_c(\mathbf{r}_\mu)$ was calculated by DFT for each of these random configurations within a $3 \times 3 \times 3$ supercell for Fe, Co

and Ni and $2 \times 2 \times 2$ supercell for MnGe and MnSi, with other computational details identical to those reported in Ref. [6].

Table II and Fig. 4 show the calculated contact field $B_c(\mathbf{r}_\mu^{eq})$ for a point-like muon [6] and its *averaged* $\langle B_c \rangle$ values, together with the experimental values. The contact hyperfine field including quantum correction within the SSCHA produces an improved agreement with experiments. This indicates the importance of the finite muon wavefunction when computing muon interactions. Notice that $|\langle B_c \rangle|$ is always smaller than $|B_c(\mathbf{r}_\mu^{eq})|$, with a reduction that ranges between 1 and 18%. However, even though the muon has large ZPE, the effect of the wavefunction spread on the contact hyperfine field is not very pronounced in the metals considered.

TABLE II. Calculated contact hyperfine field at the equilibrium muon position $B_c(\mathbf{r}_\mu^{eq})$, B_c averaged over the spread of the muon wavefunction $\langle B_c \rangle$ and experimental values.

| Host metals | $B_c(\mathbf{r}_\mu^{eq})$ [T] ^a | $\langle B_c \rangle$ [T] | Exp |
|---------------------|---|---------------------------|-------------|
| Fe-bcc ^b | -1.25 | -1.07 | -1.11 [54] |
| Fe-bcc ^c | -1.22 | -1.13 | -1.11 [54] |
| Co-hcp | -0.79 | -0.64 | -0.61 [55] |
| Co-fcc | -0.73 | -0.68 | -0.58 [50] |
| Ni-fcc | -0.15 | -0.14 | -0.071 [56] |
| MnGe | -1.14 | -1.07 | -1.08 [57] |
| MnSi | -0.22 | -0.21 | -0.207 [58] |

^a Ref. [6]

^b Muon at the tetrahedral site

^c Muon at the octahedral site

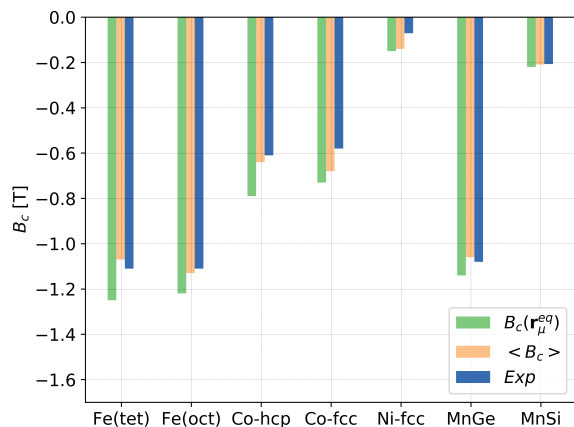


FIG. 4. Contact hyperfine field $B_c(\mathbf{r}_\mu^{eq})$ at the equilibrium muon implantation position \mathbf{r}_μ^{eq} , the muon contact field averaged over the muon wavefunction spread, $\langle B_c \rangle$ and experimentally observed values.

VI. CONCLUSION

In conclusion, we have presented a general, effective and robust approach, based on the DBO, to obtain the ground state wavefunction and ZPE of a positive muon embedded in a crystal from first principles. The adaptation of the SSCHA to the muon case allows to evaluate the delocalized muon wavefunction including anharmonic contributions, that substantially correct harmonic ones.

Moreover, the SSCHA circumvents the problem of directly reconstructing the PES by replacing this task with a variational problem, and more importantly, provides a computationally tractable method to describe the ZPE of the muon. This leads to a number of important insights concerning the stability of the muon sites and its coupling with the surrounding electrons.

The first point has been discussed by considering the case of the muon site in Fe, where anharmonicity plays a crucial role in establishing the stability of the muon in the tetrahedral and octahedral sites.

We reformulated the calculation of the muon contact hyperfine field by including the effects of its anharmonic ZPV, improving the agreement with experiments with respect to previous estimates based on the point impurity treatment of the muon. Even though the correction is small, in numerous cases the contact field is of the order of tenths of Tesla, thus making the absolute value of the correction presented here quite relevant.

Finally, the clean iterative procedure of the SSCHA makes it rather straightforward to define standardized workflows to automate the computational procedure. This represents another step towards routinely supporting experimental data analysis with computational simulation results.

ACKNOWLEDGMENTS

RDR acknowledges grants from the European Union's Horizon 2020 research and innovation program under Grant Agreement No. 654000. RDR, PB and IJO also acknowledge computing resources provided by, the Swiss National Supercomputing Centre (CSCS) under Project ID sm16, CINECA under Project ID IsC58, the STFC Scientific Computing Departments SCARF cluster and the HPC resources at the University of Parma, Italy. IE acknowledges funding from the Spanish Ministry of Economy and Competitiveness (FIS2016-76617-P). This work is part of the PhD thesis of IJO at the University of Parma, Italy.

REFERENCES

- [1] M. M. J.Rath, P.Jena, and C. Wang, *Solid State Communications* **31**, 1003 (1979).
- [2] J. S. Möller, P. Bonfá, D. Ceresoli, F. Bernardini, S. J. Blundell, T. Lancaster, R. D. Renzi, N. Marzari,

- I. Watanabe, S. Sulaiman, and M. I. Mohamed-Ibrahim, *Physica Scripta* **88**, 068510 (2013).
- [3] J. S. Möller, D. Ceresoli, T. Lancaster, N. Marzari, and S. J. Blundell, *Phys. Rev. B* **87**, 121108 (2013).
- [4] F. Bernardini, P. Bonfà, S. Massidda, and R. De Renzi, *Phys. Rev. B* **87**, 115148 (2013).
- [5] P. Bonfà and R. De Renzi, *J. Phys. Soc. Jpn* **85**, 091014(10 pages) (2016).
- [6] I. J. Onuorah, P. Bonfà, and R. De Renzi, *Phys. Rev. B* **97**, 174414 (2018).
- [7] L. Liborio, S. Sturniolo, and D. Jochym, *The Journal of Chemical Physics* **148**, 134114 (2018), <https://doi.org/10.1063/1.5024450>.
- [8] F. R. Foronda, F. Lang, J. S. Möller, T. Lancaster, A. T. Boothroyd, F. L. Pratt, S. R. Giblin, D. Prabhakaran, and S. J. Blundell, *Phys. Rev. Lett.* **114**, 017602 (2015).
- [9] P. Dalmas de Rotier, A. Yaouanc, A. Amato, A. Maisuradze, D. Andreica, B. Roessli, T. Goko, R. Scheuermann, and G. Lapertot, *Quantum Beam Science* **2** (2018), 10.3390/qubs2030019.
- [10] M. Born and R. Oppenheimer, *Annalen der Physik* **84**, 457 (1927).
- [11] M. A. Boxwell, T. A. Claxton, and S. F. J. Cox, *J. Chem. Soc., Faraday Trans.* **89**, 2957 (1993).
- [12] A. R. Porter, M. D. Towler, and R. J. Needs, *Phys. Rev. B* **60**, 13534 (1999).
- [13] C. P. Herrero, R. Ramírez, and E. R. Hernández, *Phys. Rev. B* **73**, 245211 (2006).
- [14] P. Bonf, F. Sartori, and R. De Renzi, *The Journal of Physical Chemistry C* **119**, 4278 (2015).
- [15] M. Tachikawa, K. Mori, H. Nakai, and K. Iguchi, *Chemical Physics Letters* **290**, 437 (1998).
- [16] H. Nakai, *International Journal of Quantum Chemistry* **86**, 511 (2001), <https://onlinelibrary.wiley.com/doi/pdf/10.1002/qua.1106>.
- [17] S. P. Webb, T. Iordanov, and S. Hammes-Schiffer, *The Journal of Chemical Physics* **117**, 4106 (2002), <https://doi.org/10.1063/1.1494980>.
- [18] A. Kerridge, A. H. Harker, and A. M. Stoneham, *Journal of Physics: Condensed Matter* **16**, 8743 (2004).
- [19] G. N.I. and G. E. K., *Philos Trans A Math Phys Eng Sci.*, 4372(2011) (2014).
- [20] R. Valladares, A. Fisher, and W. Hayes, *Chemical Physics Letters* **242**, 1 (1995).
- [21] M. Probert and M. Glover, “Ab initio path integral molecular dynamics simulation of hydrogen in silicon,” in *Hydrogen in Matter*, edited by G. Myneni and B. Hjorvarsson (Amer. Inst. Physics, 2006) p. 311.
- [22] I. Errea, M. Calandra, and F. Mauri, *Phys. Rev. Lett.* **111**, 177002 (2013).
- [23] I. Errea, M. Calandra, and F. Mauri, *Phys. Rev. B* **89**, 064302 (2014).
- [24] R. Bianco, I. Errea, L. Paulatto, M. Calandra, and F. Mauri, *Phys. Rev. B* **96**, 014111 (2017).
- [25] L. Monacelli, I. Errea, M. Calandra, and F. Mauri, *Phys. Rev. B* **98**, 024106 (2018).
- [26] I. Errea, M. Calandra, C. J. Pickard, J. Nelson, R. J. Needs, Y. Li, H. Liu, Y. Zhang, Y. Ma, and F. Mauri, *Phys. Rev. Lett.* **114**, 157004 (2015).
- [27] M. Leroux, I. Errea, M. Le Tacon, S.-M. Souliou, G. Garbarino, L. Cario, A. Bosak, F. Mauri, M. Calandra, and P. Rodière, *Phys. Rev. B* **92**, 140303 (2015).
- [28] I. Errea, M. Calandra, C. J. Pickard, J. R. Nelson, R. J. Needs, Y. Li, H. Liu, Y. Zhang, Y. Ma, and F. Mauri, *Nature* **532**, 81 (2016).
- [29] G. A. S. Ribeiro, L. Paulatto, R. Bianco, I. Errea, F. Mauri, and M. Calandra, *Phys. Rev. B* **97**, 014306 (2018).
- [30] U. Aseginolaza, R. Bianco, L. Monacelli, L. Paulatto, M. Calandra, F. Mauri, A. Bergara, and I. Errea, *Phys. Rev. Lett.* **122**, 075901 (2019).
- [31] R. Bianco, I. Errea, L. Monacelli, M. Calandra, and F. Mauri, arXiv e-prints, arXiv:1902.00662 (2019), arXiv:1902.00662 [cond-mat.mtrl-sci].
- [32] A. V. Soudackov and S. Hammes-Schiffer, *Chemical Physics Letters* **299**, 503 (1999).
- [33] A. Isihara, *Journal of Physics A: General Physics* **1**, 539 (1968).
- [34] J. K. L. MacDonald, *Phys. Rev.* **43**, 830 (1933).
- [35] M. R. Hestenes and E. Stiefel, *Journal of research of the National Bureau of Standards* **49**, 409 (1952).
- [36] G. Lang, K. Karch, M. Schmitt, P. Pavone, A. P. Mayer, R. K. Wehner, and D. Strauch, *Phys. Rev. B* **59**, 6182 (1999).
- [37] B. Rousseau and A. Bergara, *Phys. Rev. B* **82**, 104504 (2010).
- [38] I. Errea, B. Rousseau, and A. Bergara, *Phys. Rev. Lett.* **106**, 165501 (2011).
- [39] W. Kohn and L. J. Sham, *Phys. Rev.* **140**, A1133 (1965).
- [40] V. Fock, *Zeitschrift für Physik* **61**, 126 (1930).
- [41] D. R. H. F. R. S, *Reports on Progress in Physics* **11**, 113 (1947).
- [42] J. C. Slater, *Phys. Rev.* **81**, 385 (1951).
- [43] G. Kresse, J. Furthmüller, and J. Hafner, *EPL (Europhysics Letters)* **32**, 729 (1995).
- [44] K. Parlinski, Z. Q. Li, and Y. Kawazoe, *Phys. Rev. Lett.* **78**, 4063 (1997).
- [45] S. Baroni, S. de Gironcoli, A. Dal Corso, and P. Giannozzi, *Rev. Mod. Phys.* **73**, 515 (2001).
- [46] P. Giannozzi, S. Baroni, N. Bonini, M. Calandra, R. Car, C. Cavazzoni, D. Ceresoli, G. L. Chiarotti, M. Cococcioni, I. Dabo, A. Dal Corso, S. de Gironcoli, S. Fabris, G. Fratesi, R. Gebauer, U. Gerstmann, C. Gougoussis, A. Kokalj, M. Lazzeri, L. Martin-Samos, N. Marzari, F. Mauri, R. Mazzarello, S. Paolini, A. Pasquarello, L. Paulatto, C. Sbraccia, S. Scandolo, G. Sclauzero, A. P. Seitsonen, A. Smogunov, P. Umari, and R. M. Wentzcovitch, *Journal of Physics: Condensed Matter* **21**, 395502 (19pp) (2009).
- [47] P. Pulay, *Molecular Physics* **17**, 197 (1969).
- [48] A. Seeger, *Physics Letters A* **58**, 137 (1976).
- [49] H. Graf, G. Balzer, E. Recknagel, A. Weidinger, and R. I. Grynspan, *Phys. Rev. Lett.* **44**, 1333 (1980).
- [50] B. Lindgren and D. E. Ellis, *Phys. Rev. B* **26**, 636 (1982).
- [51] S. Estreicher and P. F. Meier, *Phys. Rev. B* **25**, 297 (1982).
- [52] E. Yagi, G. Flik, K. Fürderer, N. Haas, D. Herlach, J. Major, A. Seeger, W. Jacobs, M. Krause, M. Krauth, H. J. Munding, and H. Orth, *Phys. Rev. B* **30**, 441 (1984).
- [53] W. J. Kossler, M. Namkung, B. Hitti, Y. Li, J. Kempton, C. E. Stronach, L. R. Goode, W. F. Lankford, B. D. Patterson, W. Kündig, and R. I. Grynspan, *Phys. Rev. B* **32**, 293 (1985).
- [54] N. Nishida, R. S. Hayano, K. Nagamine, T. Yamazaki, J. H. Brewer, D. M. Garner, D. Fleming, T. Takeuchi, and Y. Ishikawa, *Solid State communications* **22**, 235 (1977).
- [55] H. Graf, W. Kündig, B. D. Patterson, W. Reichart,

- P. Roggwiler, M. Camani, F. N. Gygax, W. Rüegg, A. Schenck, H. Schilling, and P. F. Meier, *Phys. Rev. Lett.* **37**, 1644 (1976).
- [56] H. Graf, E. Holzschuh, E. Recknagel, A. Weidinger, and T. Wichert, *Hyperfine Interactions* **6**, 245 (1979).
- [57] N. Martin, M. Deutsch, F. Bert, D. Andreica, A. Amato, P. Bonfà, R. De Renzi, U. K. Rößler, P. Bonville, L. N. Fomicheva, A. V. Tsyvashchenko, and I. Mirebeau, *Phys. Rev. B* **93**, 174405 (2016).
- [58] A. Amato, P. Dalmas de Réotier, D. Andreica, A. Yaouanc, A. Suter, G. Lapertot, I. M. Pop, E. Morenzoni, P. Bonfà, F. Bernardini, and R. De Renzi, *Phys. Rev. B* **89**, 184425 (2014).